SCC Publishing
Michelets vei 8 B
1366 Lysaker Norway

ISSN: 2703-9072

Correspondence:
aveollila@ yahoo.com

Vol. 5.3 (2025)
pp. 186-210

Radiative Forcing of Water Vapour and its Use in Climate Models

Antero Ollila

School of Engineering (Emer.), Aalto University, Espoo, Finland

Abstract

The positive feedback of water vapour has been the basic feature of General Circulation Models (GCMs), which approximately doubles the warming impacts of any other climate drivers. Some published scientific papers have shown that simple climate models without this feature can simulate the temperatures of the 2000s very well. On the other hand, the observed humidity observations revealed that it varies, but not according to the water feedback theory. There is a need for an optional method for calculating the warming impacts of water vapour. In this study, the radiative forcing (RF) value of water vapour for different atmospheric water amounts has been calculated by applying the line-by-line (LBL) method. A simple climate model by the author has been modified by implementing this dependency in the same way as for the other greenhouse (GH) gases. This model has been used for the simulations of absolute yearly temperature and humidity changes, as well as for decadal-long changes by applying CERES (Clouds and the Earth's Radiant Energy System) observations. These simulations reveal that humidity increases are strongly related to the primary energy changes of the absorbed solar radiation (ASR). The yearly temperature variations of the hemispheres show that water vapour increase has about a 14 % temperature impact and not about 100 % as assumed by the water feedback theory. This water vapour RF effect explains good results in simulating the high temperatures of the 2000s. The recent rapid warming during the 2000s is mainly caused by ASR variations, and this new calculation method can be applied in temperature simulations.

Keywords: Positive water feedback**;** RF of water vapour; absorbed solar radiation; natural climate drivers; simple climate models; warming in the 2000s.

Submitted 2025-06-18. Accepted 2025-12-6. https://doi.org.10.53234/scc202510/11

1. Introduction

1.1 The solar activity changes over the 1850 – present period

In the temperature simulations of the 2000s in this study, the role of the absorbed solar radiation (ASR) turns out to be significant. Therefore, it has been considered useful to carry out a short survey of research studies about solar activity changes over the period that the IPCC has applied in its own simulations by GCMs (General Climate Models) and in the CMIP6 (Coupled Model

Intercomparison Project Phase 6) simulations.

Connolly et al. (2021) have carried out a comprehensive study consisting of 16 TSI and 5 temperature datasets. The TSI dataset included high-variability TSI estimates as well as low-variability datasets. Among the low-variability datasets is that of Matthes et al. (2017), which has been recommended to be applied in the CMIP6 simulations, and it is in line with the IPCC's general conclusion about the solar variation impacts being insignificant, as slow as ± 0.01 ºC (IPCC, 2021).

The results of Connolly et al. (2021) show that, applying high-variability TSI datasets like those of Hoyt & Schotten (1993) and Bard et al. (2000), most of the NH warming trend since the 19th century can be related to solar variability.

Stefani (2021) applied the multiregression method to correlate solar activity and logarithmic CO_2 concentration to sea surface temperature variations from 1850 to 2018. The geomagnetic aa index was applied as a proxy for solar activity changes. The correlation R^2 value of around 0.87 was for a climate sensitivity (of TCR type) in the range of 0.6 K to 1.6 K per doubling of CO_2. By eliminating the data of the last decade, the regression produced a significantly higher weight of the aa index.

Scafetta (2023) applied an energy balance model calibrated with a differential multilinear regression method in simulating the global temperature response from 1850 to 2020. He used anthropogenic, volcanic and solar climate drivers. As the solar proxies, he used three balanced multi-proxy TSI datasets combined from high-variability TSI records and the record of Matthes et al. (2017) as a reference, since it has been applied by the IPCC. The simulation results show that greater TSI variability matches more closely with the temperature records, implying that the ECS should be from 1.4 ºC to 2.8 ºC with a mean of 2.1 ºC.

Harde (2022) has applied his energy-radiation-balance model for the simulation of global temperature. He has integrated into his model the same feedbacks as in the CMIP6 model, and in addition to these, also convection and evaporation feedbacks. The best simulation result with a correlation factor of r = 0.95 was achieved with the ECS value of 0.68 °C and the TSI dataset of Hoyt & Schatten (1993). A convincing feature of this simulation was the accurate reproduction of the temperature peak of the 1930s and the strong temperature drop from the 50s to 80s.

It can be summarised that the published high-variability TSI estimates outnumber the low-variability TSI estimates, and the different types of analyses show that in simulations, they reproduce the observed temperature trends with much better accuracy than the low-variability TSI dataset applied in the CMIP6 simulations.

1.2 The theory of positive water feedback applied by the IPCC

GCMs have an essential role in calculating global surface temperature changes. Manabe & Wetherald (1967) were the first to introduce positive water feedback. Their calculations showed only that water feedback doubles the original RF of CO_2. The consequence of this feature was the λ value of the climate sensitivity parameter of 0.53 K/(Wm^{-2}) in their study. Without positive water feedback, the λ value is about 0.27 K/(Wm^{-2}) as shown by Ollila (2023b). Manabe & Wetherald (1967) did not show that water feedback is a persistent property of the climate, even though many climate researchers think so. This feature became one of the essential features of GCMs already in the 1980s.

Positive water feedback is a cornerstone in any GCM and the simple model applied by the IPCC. The IPCC (2007) writes in AR4 that "*The positive water feedback doubles the radiative forcing of any GH gas".* The AR5 (IPCC 2013, p. 667) writes *"Therefore, although CO_2 is the main control knob on climate, water vapour is a strong and fast feedback that amplifies any initial forcing by a typical factor between two and three."* The fast feedback means that the response happens on the same timescale as any climate driver, and like CO_2 warms up the surface. The typical lifetime of water vapour in the atmosphere is about ten days.

The theoretical justification of positive water feedback is based on the equation of Clausius-Clapeyron (C-C), and this relationship has been referred to 36 times in AR6 (IPCC, 2021) as an explanation of water feedback in the lower atmosphere. This equation represents the pressure-temperature relationship in a saturated water vapour atmosphere. The C-C relation states that a 1-degree increase raises the water-holding capacity of the atmosphere by 6-7%. The actual amount of water in the atmosphere is given by the water-holding capacity times the relative humidity of the atmosphere. The real atmosphere is not saturated by water vapour, since the atmospheric humidity is around 70% and it varies greatly in different climate zones. Therefore, the theoretical basis is weak.

The C-C equation presupposes that there is enough energy to evaporate water while maintaining 100 % saturation in the gaseous atmosphere. This is not the case in the atmosphere.

The direct humidity and temperature measurements from 1980 onwards show no positive water feedback in the long run (Fig. 1). Reliable empirical conclusions about the water feedback can be drawn from the behaviour of the climate since 1979, after the worldwide use of the new humidity semiconductor technology Humicap® of Vaisala.

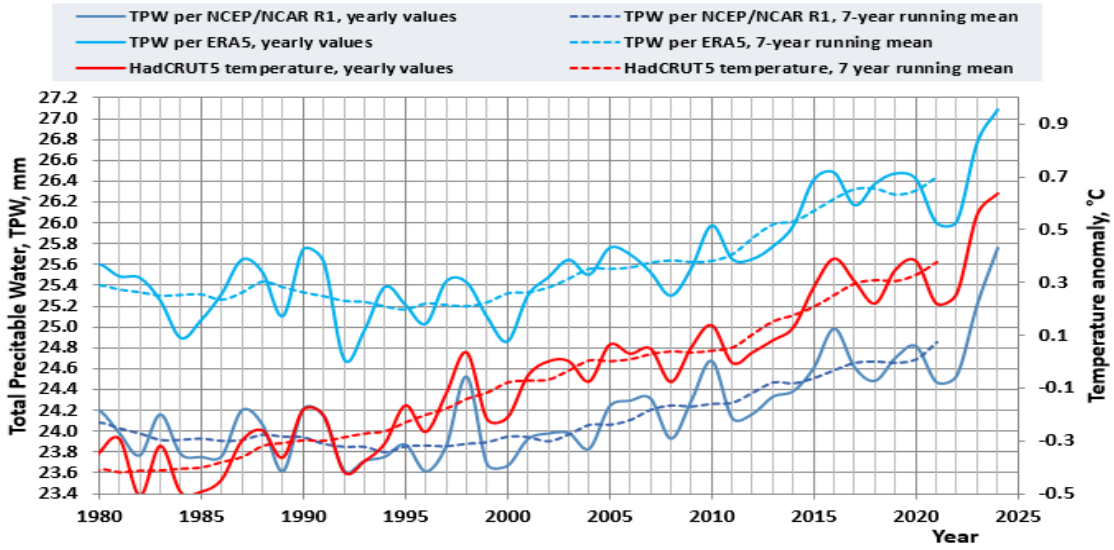

Figure 1: The temperature trend (MetOffice, 2025) and Total Precipitable Water (NOAA, 2025a) trends according to two humidity measurements from 1980 to 2024. ERA5 stands for the fifth generation of the European Centre for Medium-Range Weather Forecasts (ECMWF) reanalysis for the global climate and weather. The NCEP/NCAR reanalysis is a joint project between the National Centers for Environmental Prediction (NCEP) and the National Center for Atmospheric Research (NCAR) in the United States.

Wang et al. (2020) carried out an accuracy analysis on the five commonly used absolute humidity

measurement data sets (precipitated water in millimetres = total precipitable water = TPW). They found that the smallest root mean square error of 1.45 mm was in JRA5 data, and the greatest was 3.34 mm in the NCEP/NCAR dataset for the period from 2016 to 2018 (NOAA 2025b). In the later analyses of this study, the humidity values of ERA5 have been applied.

These data sets have been depicted in Fig. 1 as yearly and 7-year running mean values. It can be noticed that the long-term value of temperature has increased by about 0.8 ºC from 1979 to 1994, but both TPW graph values show a negative trend (a 7-year running mean). These empirical trends of TPW versus temperature conflict with the positive water feedback theory. Trenberth et al. (2015) found that the three-dimensional Community Earth System Model (CESM), calculating a global surface mean temperature (GSMT) increase of 0.4 ºC from 2000-2014, was significantly greater than the observed 0.12 ºC. They concluded that the temperature pause was still a reality at the end of 2014. During the temperature pause, both TPW values showed a positive trend. Since 2014, both the temperature and TPW values have increased significantly, and in this sense, it is in line with the water feedback theory. The reasons for this change will be analysed later.

It is the common principle of science that a theory or a paradigm must pass through any experiment or test. Albert Einstein experienced a lot of criticism for his new theory of relativity. He responded to critics: "*No amount of experimentation can ever prove me right; a single experiment can prove me wrong.*" This same applies to the paradigm of positive water feedback applied by the IPCC.

1.3 Studies of water feedback and greenhouse effect magnitude by dissenting researchers

Harde (2014; 2017) has carried out a theoretical analysis of the magnitudes of water vapour feedback based on the spectral lines of water and CO_2, which have overlapping absorption regions. He realises that the water spectral lines are already strongly saturated in the same way as CO_2 in this region. Therefore, by increasing water concentration, only the far wings of its spectral lines and weak absorption bands can further contribute to an additional absorption, which increases roughly logarithmically with the water vapour concentration. Water vapour concentration increases exponentially with rising temperature, but due to the C-C relation, the overall effect results in a linear increase in the absorptivities. Harde concluded that the water vapour feedback amplification is only 1.14 or 14 %, and not 2 or even more as reported by the IPCC in the AR5 (IPCC 2013). Harde (2022) applied this water feedback in his TSI and CO_2 simulations with good results.

Koutsoyiannis (2024) has carried out a comprehensive study about the GH effect and the magnitude of its contributors. The results based on MODTRAN calculations and mathematical analyses show that the contribution of CO_2 is 4 % – 5 %, and water and clouds dominate with a contribution of 87 % – 95 %. These results can be compared to other results, which are surprisingly few.

Schmidt et al (2010) have reported the CO_2 contribution as 19 %. Their calculation method is exceptional, since it is an average of two calculations: absorption change by removing CO_2 from the atmosphere, and calculating the absorption increase if CO_2, as it is the only GH gas in the atmosphere. The most common procedure is a so-called "single factor removal", which means that each GH gas has been removed from the atmospheric composition, and the reduced absorption amount is calculated for the total absorption in the atmosphere. The CO_2 contributions calculated with this method and applying the total absorption of 155-159 Wm^{-2} of the terrestrial

radiation are very close to each other: Schmidt et al. (2010) 14,9 %, Harde (2017) 15 %, and Ollila (2017) 14.9 %.

Ollila (2019) has found that the IPCC (2013; 2021) has its own definitions of the GH effect, which are not based on any scientific publication. He has proposed a new definition for the magnitude of the GH effect. It is based on the Earth's energy balance, which shows that the surplus of radiation energy on the surface in comparison to the net energy input from the sun is 510 Wm^{-2} - 240 Wm^{-2} = 270 Wm^{-2}. By applying this figure, the contribution of CO_2 to the GH effect is only 7.4 %.

Koutsoyiannis (2024) has also calculated the relative strengths of water over CO_2 based on impacts on the upward and downward LW radiation changes in the atmosphere, and the corresponding values are 9.1 and 13.8, which means an average value of 11.9. It is interesting to note that the same value of Ollila (2017) is 11.8 based on the LW absorption in the atmosphere. It should be noted that the contribution calculations in the GH effect consider the total impact of a GH gas from its zero concentration to the present-day value. The relative strength calculations consider only relatively small concentration changes – typically 10 % increase - from the present values. Especially, the RF value of CO_2 is very nonlinear, but the water vapour RF value is close to linear dependency.

These different analyses show that the research studies of dissenting researchers concerning the strength and role of water and CO_2 deviate remarkably from the mainstream results.

1.4 Research study theories of the warming in the 2000s

The temperature trend of the 2000s shows that there has been a so-called temperature pause from 2000 to 2014 and thereafter a relatively strong warming period with record-high temperatures in 2023 - 2024. Many different theories have been proposed for the reasons for the pause, and in the same way, different theories have been proposed for the present warming after 2014, since the GH gases cannot explain the present warming.

Loeb et al. (2018) found a significant reduction of 0.83 Wm^{-2} in global mean reflected SW flux at the TOA during the years 2014 - 2017. Ollila (2020) used the same CERES observations and identified that the SW anomaly forcing caused about 50 % of the El Niño temperature impact of 2015-2016. Ollila (2021) noticed that the GCMs can simulate current temperatures only if the SW anomaly of the 2000s has been omitted.

Harde (2022) has summarised research studies on the complicated nature of cloud feedback with observations that it is positive over the Pacific due to low-level cloud impacts and negative in the tropics. He has been able to formulate a mathematical equation connecting the cloud cover dependency on the TSI. Svensmark (2019) developed a comprehensive model about the mechanism between solar activity variations and cosmic radiation, which changes cloud formation through the generation rate of aerosols as water vapour condensation nuclei.

The later study of Loeb et al. (2021) has confirmed the earlier finding of Loeb et al. (2018) that low-level cloud reduction (the reduced albedo) has been the reason for increased ASR. Ollila (2023a) and Nikolev and Zeller (2024) have shown that the ASR anomaly variations can explain the major part of the temperature variations of the 2000s.

During the last few years, some research studies have been published, in which a common feature has been to identify anthropogenic reasons for the reduced albedo of the Earth. Due to new legislation, the sulphur emissions from the shipping industry have reduced, and the impacts have been at a maximum of 0.1 Wm^{-2} according to Diamond (2023) and from 0.02 to 0.06 Wm^{-2} according to Rantanen and Laaksonen (2024).

Hodnebrog et al. (2024) recognised the substantial diversity in aerosol Effective Radiative Forcing (ERF) among Coupled Model Intercomparison Project phase 6 (CMIP6) GCM models. For example, the decline of SO_2 emissions in China after 2007 is not accounted for in the earlier GCM simulations. They carried out a multi-model multi-ensemble approach, and they found that the ERF due to anthropogenic aerosol emission reductions has led to a 0.2 ± 0.1 Wm^{-2} $decade^{-1}$ strengthening of the 2001–2019 imbalance trend.

Since the reduction of SO_2 aerosol has been the most significant in China, the temperature trends in China and the global temperature trend are depicted in Fig. 2.

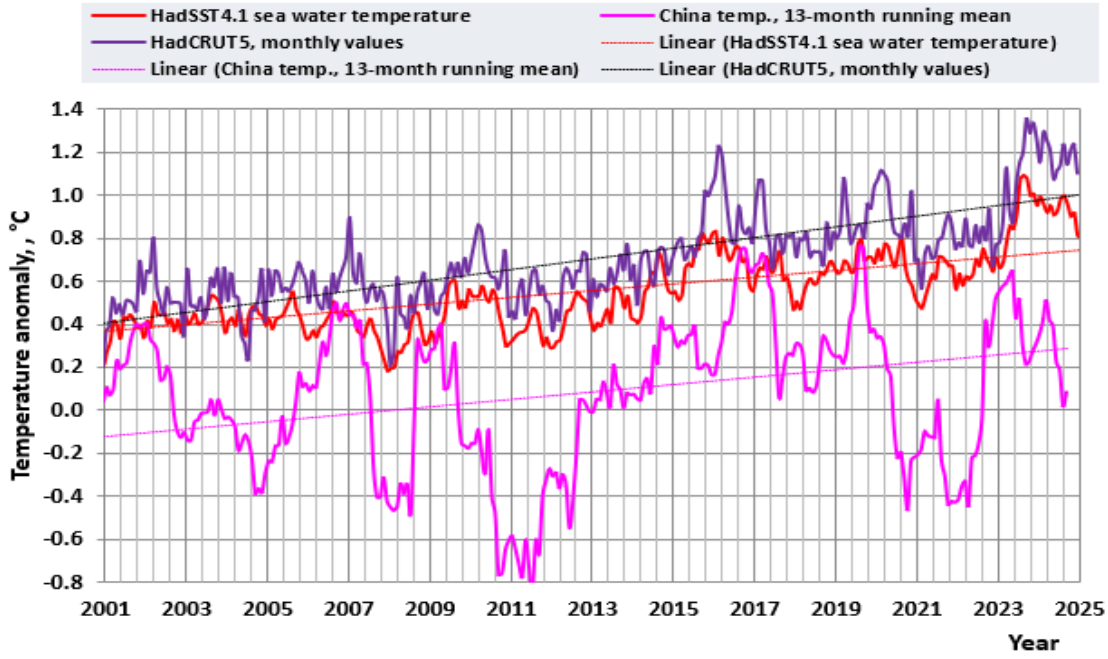

Figure 2: The global temperature trend (MetOffice, 2024), the seawater temperature trend, HadSST.4.1 (Metoffice, 2025) and the temperature trend over China (NOAA, 2025b).

The fluctuations of temperature trends in China are much greater than those in global temperatures, but the linear increase during the last 10 years is similar to the global sea surface temperature. Since the fluctuations are so great, some other factors are more probable reasons for temperature fluctuations than the aerosol reductions.

The Hunga Tonga–Hunga Ha'apai submarine volcano eruption of magnitude VEI-5 in January 2022 created a strong water and ash plume reaching the stratosphere. Rantanen and Laaksonen (2024) have estimated the radiative warming effects of this eruption to be from 0.02 to 0.07 Wm^{-2}, and the estimate of Hansen et (2025) was negative, of -0.3 Wm^{-2}. Gupta et al. (2025) have studied in detail the water and sulphate impacts in the stratosphere, and they found that sulphates themselves and sulphate aerosols' interactions with humidity deplete the ozone layer, which leads to cooling. The net effect of the eruption was estimated to be -0.10 ± 0.02 K in the southern hemisphere. It means that opposite results have been achieved.

Raghuraman et al. (2025) have shown that climate models have such a large internal variability that they can simulate high-temperature spikes, which happened in 1976 - 1977 and 2022 - 2023, without external forcing or changes in GH gas concentrations or aerosols. These events happened under special conditions connected to the change from the La Niña to the El Niño phase. It should be noted that this is a result of GCM simulations, and the real physical reason cannot be identified.

Ma et al. (2025) found that there has been a decline in ocean evaporation due to wind, even after 2017. This result is not in line with the TPW observations since the global humidity has increased steadily even after 2017 (Fig. 1), and it may be one of the explanations for the high temperatures of the years 2023 and 2024.

Myessignac et al. (2023) found that the climate feedback parameter – the reciprocal of the climate sensitivity parameter – is not constant but varies within the range from −3.2 to −1.0 $Wm^{-2}K^{-1}$ since 1970, the sea surface temperature, and is related to the phase of PDO (Pacific Decadal Oscillation). This result is in line with the information in Fig. 1. The PDO is a well-known general climate oscillation phenomenon, and there is no recognised increase of a warm phase during the 2000s, but there has been a cold phase after 2015 (NOAA 2025a).

The short-term temperature changes are distinctly related to the El Niño and La Niña events, which are caused by the regional changes of the ocean currents and winds in the tropical central and eastern Pacific Ocean. They initiate the temperature change, and the strong change in absolute humidity amplifies the change by a factor of about 100 percent of very strong El Niños (Ollila 2020). It is practically the same as the positive feedback used by the IPCC.

As we can see in the referred studies above, the proposed anthropogenic reasons are not strong in explaining the warming after the year 2015. But there is another strong climate driver, as originally found by Loeb et al. (2018), that the main reason is the reduction of the albedo, which has caused a strong increase in ASR. So far, there is no general explanation for the cloudiness decrease identified by Loeb et (2018), even though sulphate reductions have been proposed as an anthropogenic reason. Marsh and Svensmark (2000) have found a likely reason for cloudiness changes as they identified a relationship between the solar-modulated cosmic rays on global cloud cover (≤ 3 km).

The reasons for temperature changes in the 2000s are opposite to the findings of the latest reports of IPCC (2013, 2021), which show the aerosol-cloud radiation cooling effect from -0.82 Wm^{-2} in 2011 to -1.00 Wm^{-2} in 2019. A clear change happened in the 2000s, and the most common paradigm is that cloudiness now plays a major role in recent sudden temperature variations.

The main objection to using ASR as a climate driver in climate models is the claim that it is not an independent climate driver. It is well-known that ASR depends strongly on cloudiness, as shown by Loeb et al (2021). One can ask, is CO_2 an independent climate variable? It is not, since the yearly atmospheric CO_2 concentration increases only by about 45 % (IPCC 2021) in comparison to the value calculated from the actual fossil fuel emissions, but it varies yearly; the reason is deeply related to the CO_2 circulation between the atmosphere, the ocean, and the land plants. Since climate science is not capable of calculating ASR utilising cloud properties, it is well-established to use ASR as an independent climate driver for the time being. The real test can be found in temperature simulations of the short and long runs in Section 4.

These findings mean that there is a need to develop the RF value for water vapour in the same way as for the other GH gases. The author has not identified any RF equations for water, and therefore, he has carried out spectral analysis calculations to quantify the relationship between RF values and absolute humidity.

The present GCMs do not apply very well to temperature simulations of the 2000s, since they do not utilise direct CERES radiation observations and are poor at simulating ASR variations (Trenberth and Fasullo 2009; Stephens et al. 2022; IPCC 2013; IPCC 2021). The idea of GCMs has been that they should be capable of simulating also cloudiness changes, but so far, GCMs cannot do it.

Ollila (2023a) has not applied the positive water feedback in his simple climate models. Even though the water impact has been assumed to be constant, his simulation results during the 2000s are very close to the observed temperatures. This model has been named Ollila-1. In this study, a new version of Ollila-2 has been developed. The warming impact of water vapour in the Ollila-2 model is based on the RF values of water vapour, utilising the observed humidity concentrations in the atmosphere.

The objectives of this study are to develop the RF equation for atmospheric water vapour and to test the positive water feedback theory by applying the Ollila-2 model.

2. Materials and methods

2.1 Materials

The temperature data are from NOAA (2025a), HadCRUT5 and HadSST.4.1 from MetOffice (2025), Berkeley (2025), and UAH (2025). The reflected shortwave radiation data for 1980 – 2001 are from ISCCP (2025), and the TSI (Total Solar Radiation) variations from the data set of Dewitte et al. (2022). The radiation data from 2001 onward are from the CERES (2025) satellite observations. The Oceanic Niño Index (ONI 2025) is from NOAA. In temperature simulations, humidity data are from NOAA (2025b) as well, and the GH gas concentrations are from NOAA (2025c). The RF equations for CO_2, CH_4, and N_2O are from Ollila (2023b), and in the simple IPCC model, they are from the IPCC (2021). In LBL calculations, the Spectral Calculator tool of Gats Ins. (Gats 2025) was applied using the HITRAN database of version 2022 (HITRAN 2025).

2.2 Spectral Calculator application

Spectral Calculator of Gats (2025) has been used in LBL calculations to simulate water vapour and other greenhouse (GH) gas concentration changes. The high-resolution transmission molecular absorption database of the Harvard-Smithsonian Center for Astrophysics (HITRAN 2025) was applied, which includes the water continuum model 2.52 MT_CKD of Mlawer et al. (2012). The polar summer profiles of the Spectral Calculator (Gats 2021) have been modified for temperature, pressure, and GH gas concentrations to correspond to the Average Global Atmosphere (AGA) profiles. These profiles have been tabulated in Appendix A, together with the global single profiles calculated as the combination of different climate zones. Appendix B is a summary of the calculation capabilities of the Spectral Calculator.

3. The radiative forcing of water vapour

The RF values of water vapour were calculated by varying the water vapour concentration H_{TPW} from 4 mm to 41mm, and the CO_2 concentration from 330 ppm to 490 ppm. In the LBL calculations, the RF effects of water vapour are calculated based on the temperature, pressure, and water vapour concentration profiles of different climate zones, which are combined into one average climate atmospheric (AGA) profile. The H_{TPW} value is a measure of the total water vapour amount in the atmosphere, which is available in atmospheric data sets (NOAA 2025a).

The calculations show that the impact of CO_2 concentration was minimal. The RF effect between

the 330 ppm and 490 ppm was only 0.04 Wm^{-2} on the RF value of water vapour. Since this is smaller than the estimated calculation accuracy, this effect was neglected.

The RF curve of absolute humidity H_{TPW} variation from 4 to 41 mm has been depicted in Fig. 3. The fitting according to the second-order equation is (coefficient units Wm^{-2}, $Wm^{-2}mm^{-1}$, and $Wm^{-2}mm^{-2}$, respectively)

$$RF = -5.3526 + 1.5733 * H_{TPW} - 0.0156 * H_{TPW}^{\,2} \ [Wm^{-2}]. \quad (1)$$

The coefficient of determination R^2 is 0.9959, and the standard error of the fitting is 0.89 Wm^{-2}.

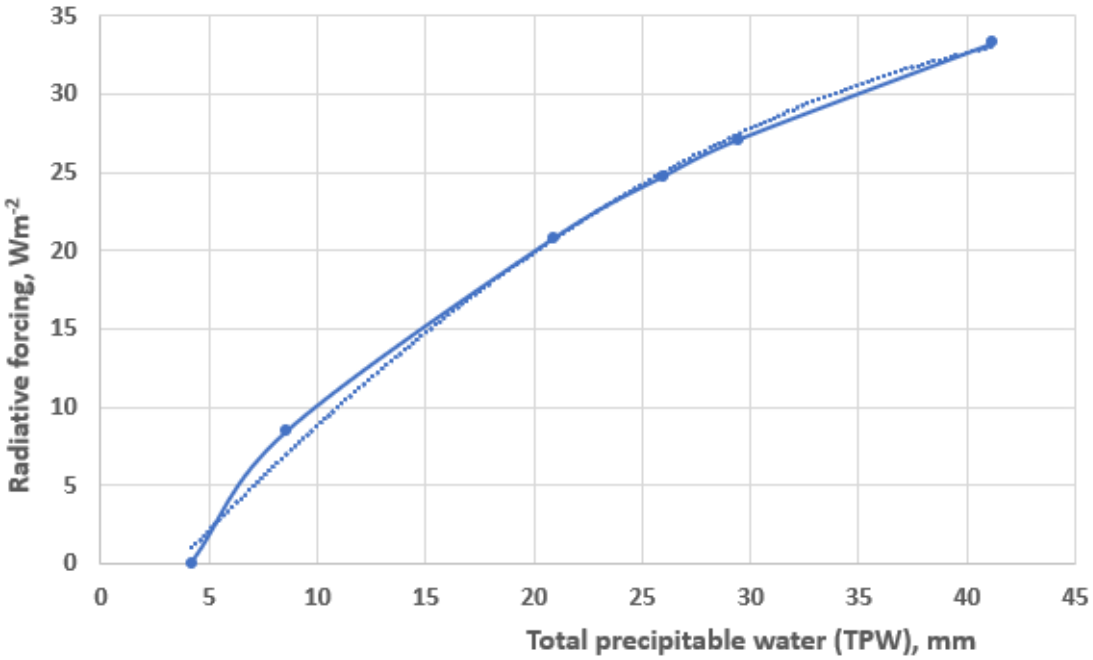

Figure 3: The RF dependency RF according to the TPW values for the range from 4 mm to 41 mm. The dotted curve is the fitted curve.

Since the H_{TPW} range in the average global climate is much smaller, another equation was calculated applicable for the H_{TPW} range from 20 mm to 30 mm, which has been depicted in Fig. 4 overleaf.

This fitting has a logarithmic dependency (coefficient units Wm^{-2}, and $Wm^{-2}\,mm^{-2}$, respectively):

$$RF = -35.304 + 18.435 * \ln(H_{TPW}) \ [Wm^{-2}]. \quad (2)$$

The dependency, according to equation (2), is practically linear, its coefficient of determination is $R^2 = 0.9999$, and the standard error of the fitting is 0.034 Wm^{-2}. These equations can partially explain why water vapour is a much stronger GH gas than CO_2. The strengths of water and carbon dioxide can be compared to each other in Fig. 5 overleaf.

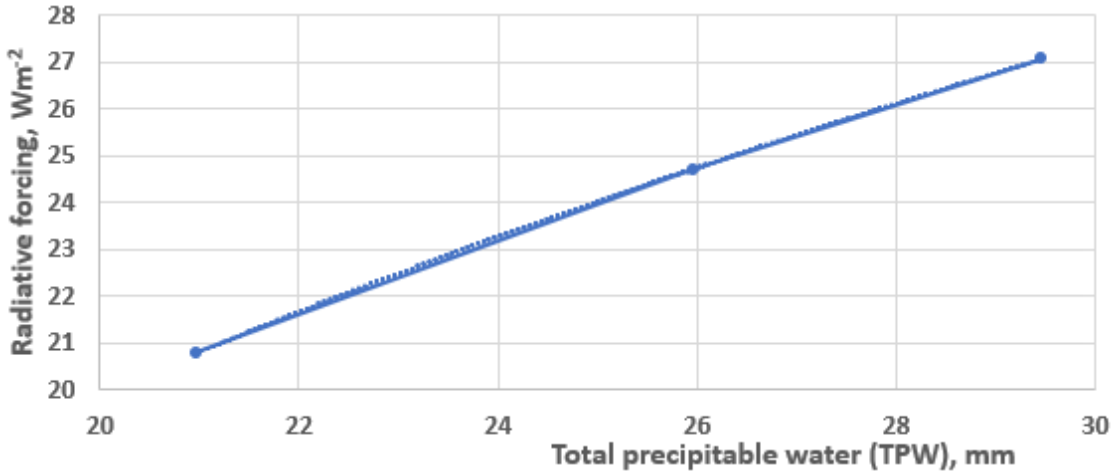

Figure 4: The RF dependency RF according to the TPW values only for the narrow range from 21.0 mm to 29.5 mm. The dotted curve is the fitted curve.

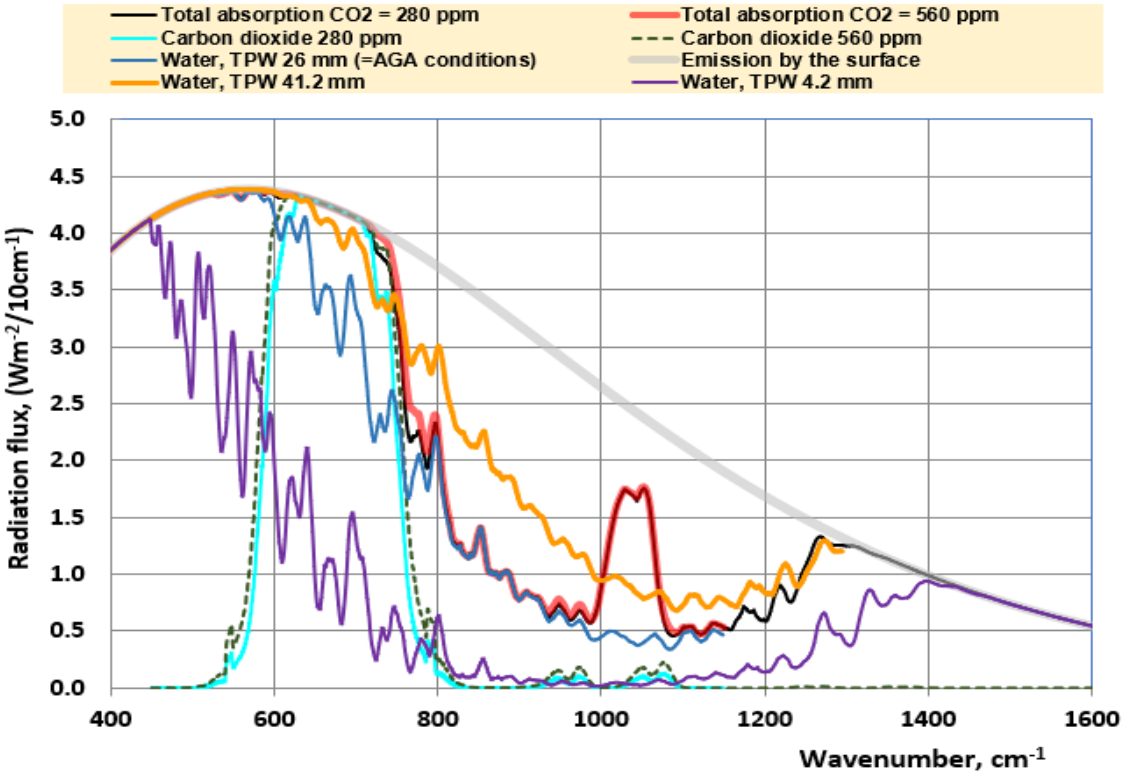

Figure 5: The absorption graphs under different atmospheric conditions under the average global atmospheric (AGA) conditions, when the surface temperature is 16.3°C (289.5 K). The CO_2 of 280 ppm (light green solid curve) and 560 ppm (dotted dark green curve) have been calculated, when CO_2 is the only GH gas in the atmosphere. The water vapour graphs of 4.2 TPW mm (purple curve), 26 mm TPW (blue curve), and 41.2 TPW mm (yellow curve) have been calculated under AGA conditions. The total absorption graphs (grey and red curves) have been calculated under AGA conditions. The emission graph corresponds to the surface temperature of 16.3 °C, assuming the emissivity factor to be 1.0.

Fig. 5 illustrates the dominant role of water vapour under the average atmospheric conditions (AGA). Under tropical conditions, the role of CO_2 is insignificant, which can be noticed by

comparing the water absorption curve (yellow) and the CO_2 absorption curve (green) to each other. The same conclusion can be drawn from total absorption curves when the CO_2 concentration increases from 280 ppm (black curve) to 560 ppm (red curve). This means a minimal warming effect of increasing CO_2 concentration in the tropical climate zone. Water vapour does not decrease significantly even in tropical conditions since its absorption increases in the wavelength zone of 7 μm - 14 μm, where the absorption effects of increasing CO_2 concentrations are much smaller.

4. Verification and validation

4.1 Verification of LBL calculations

The validations of LBL calculations are not possible due to the too-small temperature effects under real climate conditions, but verification tests are possible.

Ollila (2023b) has shown that the LBL calculations carried out under average atmospheric conditions of 2008 – 2014 (detailed in Appendix C) resulted in the OLR flux of 272.0 Wm^{-2} for the clear sky, which is almost the same as the CERES observed flux of 272.6 Wm^{-2} during the same period (Huang and Chen 2020). The GH gas effects can be found to be in the same wavelength zones in both the calculated and the satellite-observed jagged curves. These results show that LBL calculations of this study are reliable, and the correct atmospheric composition has been applied.

4.2 The simple climate models applied in temperature simulations

Three different simple climate models have been applied to temperature simulations, and they have the same common features, but the RF and temperature calculations are different.

The positive water feedback can be tested by applying simple climate models. In this study, a simple climate model has been applied as defined by IPCC (2013) on page 664

$$dTs = \lambda * RF, \quad (3)$$

where dTs is the global mean surface temperature change, and λ is the climate sensitivity parameter. The warming impacts of climate drivers, which are in this study, ASR, and GHGs, including also water vapour, can be added together. This simplification is justified for simulations based on the graphs of Fig. 7.8 of the AR6 (IPCC, 2021), which show that the warming impacts of tropospheric aerosols, halogenated gases, ozone, and volcanic aerosols have been essentially constant during the 2000s.

The dynamic delays of RF values have been calculated by applying the first-order dynamic models as specified in the studies of Ollila (2020; 2021; 2023a). In this study, all the variables and the observed temperature were normalised to zero temperature effect for the period of 2003-2008.

The essential difference between the Ollila models and the IPCC simple model is the value of λ. The warming values of all climate drivers tabulated in Figures 7.6 and 7.7 in AR6 (IPCC 2021) are possible if the λ value of 0.47 $K/(Wm^{-2})$ has been applied, which means the use of positive water feedback in the original GCM calculations.

The λ without water feedback can be calculated from the energy balance of the Earth (Ollila 2023b) according to the equation

$$\lambda = T/(SC(1-\alpha)), \quad (4)$$

T is the emission temperature of the OLR radiation, SC is the solar constant, and α is the total

albedo of the Earth. By applying the average CERES (2025) OLR flux values for the period 2008 - 2014, the SC is 1360.04 Wm^{-2}, α is 0.2916, and λ is 0.265 $K/(Wm^{-2})$. The λ value can be calculated for each month according to Eq. (4), and this has been applied in simulations of this study.

In the earlier model Ollila-1 (Ollila, 2021), the warming impact of the ENSO (El Niño and Southern Oscillation) effect was calculated by the equation first introduced by Trenberth and Fasullo (2013).

$$dT_{ENSO} = 0.1 * ONI, \quad (5)$$

where dT_{ENSO} is the warming impact of the ENSO phenomenon applying a 5-month delay, and ONI is the Oceanic Niño Index (ONI 2024). In the Ollila-2 model, the ENSO effect has been replaced by the warming impact of water calculated on the H_{TPW} basis and possible absorbed solar radiation (ASR) impacts.

In both Ollila models, the radiative forcings of CO_2, CH_4, and N_2O have been calculated by the equations developed in the study of Ollila (2023b), and the same in the IPCC simple model are calculated using the equations of AR5 (IPCC 2013). The differences in the RF values of CH_4 and N_2O are insignificant in these two cases.

In the temperature simulations, first-order dynamic models have been applied. The dynamical time constants for the ocean have been 2.74 months and for land 1.04 months (Stine et al. 2009). The responses of first-order dynamic models can be calculated in the discrete form by applying the so-called z-transform, which enables continuously changing input variables.

4.3 Water vapour warming impacts during the yearly temperature cycles

The temperature of the Earth varies in the same way each year on both hemispheres. Only after 2020 has the NH temperature been increasing more rapidly than the SH temperature, and the reason is probably the ASR increase due to cloud cover changes on the NH hemisphere (Hansen et al., 2025). The variation is much greater than the temperature anomaly measurements indicate.

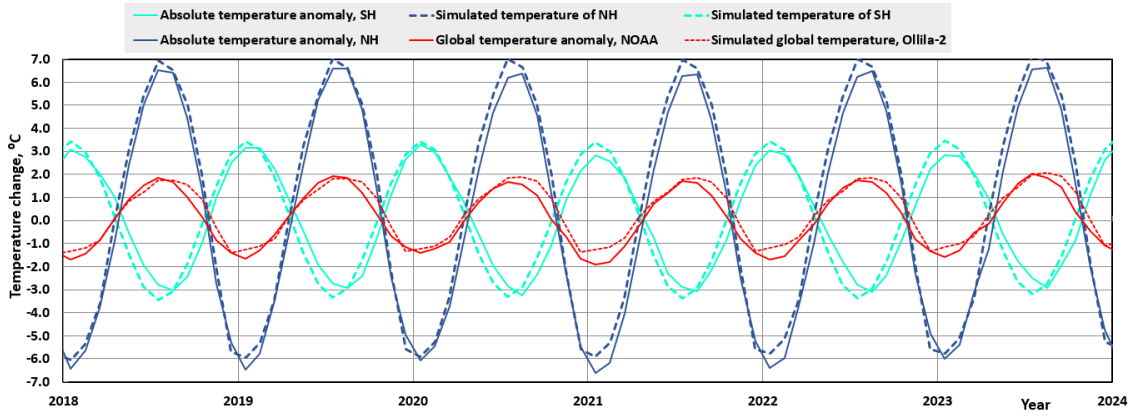

Figure 6: The graphs of the observed (NOAA, 2025b) and simulated temperature yearly changes of NH, SH and the whole Earth by the Ollila-2 model. A one-month delay in temperatures from February to June due to the melting of ice and snow cover has been applied in the simulated NH temperatures.

The global absolute temperature varies from about 12.5 °C to 16.0 °C. The variation in the northern hemisphere (NH) is much greater, from about 9.5 °C to 22.0 °C, but in the southern hemisphere (SH), from about 10.0 °C to 16.0 °C. These observed temperature graphs have been

depicted in Fig. 6, as well as the simulated temperatures by the Ollila-2 model.

The graphs show that the Ollila-2 simulates the temperatures very well, even though the simulation step is relatively long, with one month. The maximum global temperature normally happens in July, even though the globe receives about 22 Wm^{-2} more total solar radiation (TSI) in December-January than in June-July. Another decisive factor is the ratio of ocean and land. In the NH, the portion of the sea is 69 %, but in the SH it is 81 %. This means that the temperature variation is much smaller in the SH.

Since the dynamic delays and time constant differ between the hemispheres, the global temperature simulations have been carried out separately for both hemispheres, and the global simulation is the sum of these simulations (Fig. 7). The humidity changes, which should cause the positive water feedback, are fast changes happening at the same speed as the temperature changes.

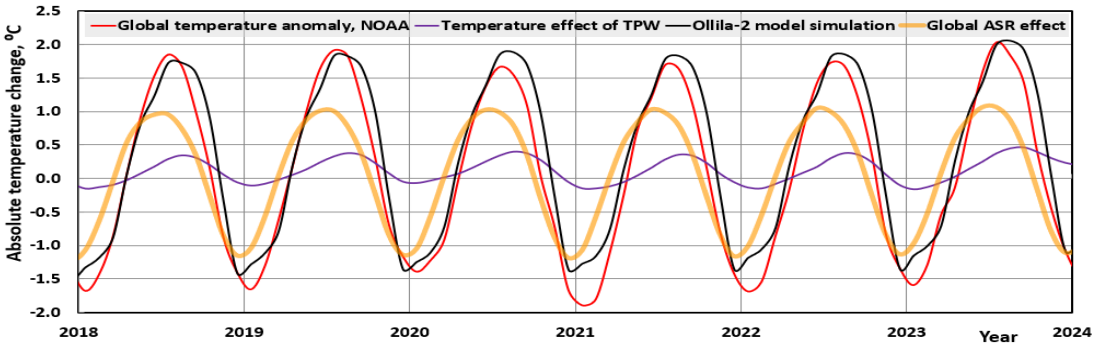

Fig. 7: The graphs of the observed (NOAA) and simulated temperature anomalies of the globe.

Also, the temperature impacts of ASR and water vapour (H_{TPW}) have been depicted. In Fig. 7, it can be noticed the fact that the ASR is the dominating climate driver of the Earth. The yearly temperature effect of GH gases according to IPCC science is only about 0.02 °C, and that is why it has not been depicted. The major finding of these simulations is that the temperature effect of water vapour variations is only from 12.8 % to 14.5% in addition to the ASR warming effect. This result is practically the same as that found by Harde (2017), that the water vapour feedback increases the climate sensitivity of the CO_2 impact by about 14 %. According to the positive water feedback theory, it should be about 100 %.

4.4 Temperature and radiation trends from 1980 onward

The paradigm of the IPCC has been that GH gases are the climate drivers since industrialisation started in 1750. The temperature effect of GH gases, according to the IPCC, has been depicted in Fig. 8 overleaf, and it has a similar linear trend as the global temperature.

On the other hand, the ASR trend has the same kind of linear trend. The fluctuations of the ASR are very great based on the ISCCP data from 1983 to 2001, but the fluctuations are much smaller during the CERES satellite measurement period, which started in 2001, indicating a better measurement accuracy. It means that further analyses are needed to find out the roles of GH gases and the ASR changes in global warming.

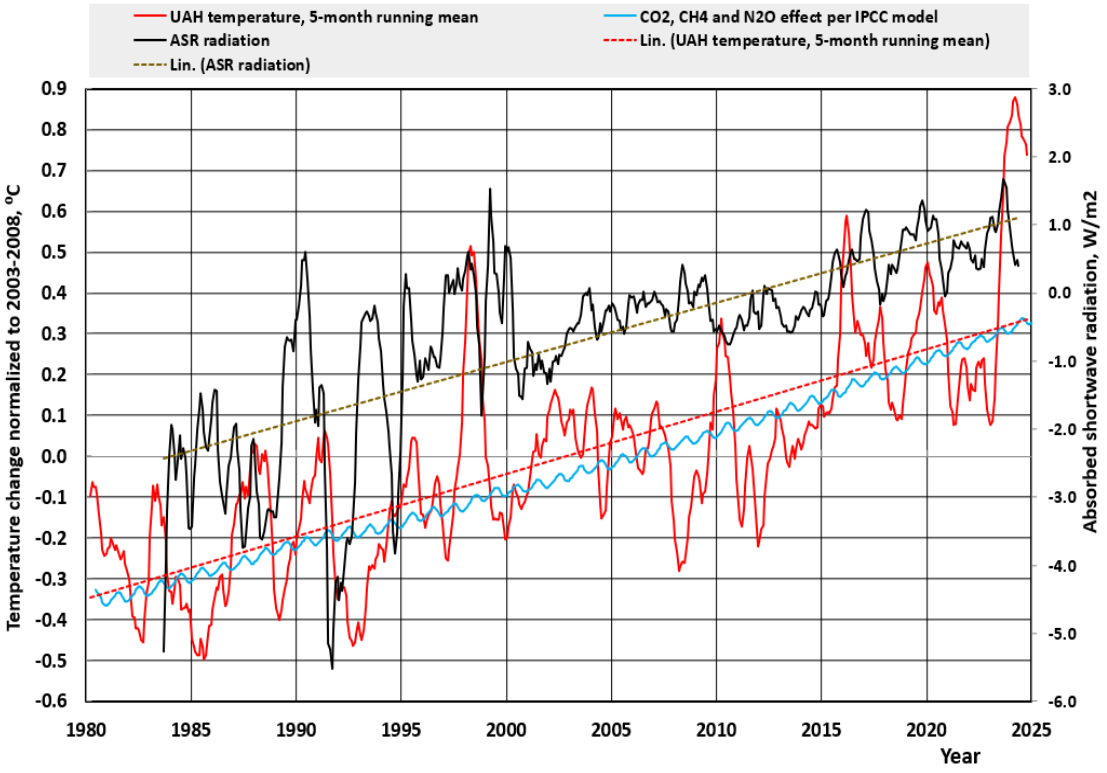

Figure 8: The temperature trend from 1980 to 2025, together with the ASR radiation trend and the temperature effect of GH gases according to the IPCC.

4.5 Water vapour warming impacts during the 2000s

The water feedback theory can be tested between 2001 and 2024, when the most accurate observations are available. The positive water feedback theory can also be expressed that any surface temperature increase should include a water vapour impact corresponding to about 50 % of the total change. The temperature and humidity observations have been depicted in Fig. 9 together with major variables. During this short simulation period, the ENSO warming impacts must be included. The warming impact of ENSO originates from the absorbed solar energy, which is released in the El Niño phase, and then during the cooling period of La Niña, this energy is paid back.

It is easy to notice that the 50 % temperature anomaly (dotted lilac curve) does not vary according to the temperature effect of GH gases as implied by the positive water feedback theory by the IPCC. It should be noticed that according to AR6, CO_2 corresponds to about 80 % of the temperature increase from 1750 to 2019 (IPCC 2021). By judging with the eye, the ASR & ENSO effect has had the dominant role in the temperature increase after the year 2014.

One of the objectives of this study was to test the theory of positive water feedback. Two observation-based analyses have been carried out. The first one was the seasonal temperature variation analyses in section 4.3, which show that the H_{TPW} temperature impact increases the absorbed solar radiation (ASR) effect by a factor of 1.14 and not by about 2 as assumed by the IPCC based on the C-C equation.

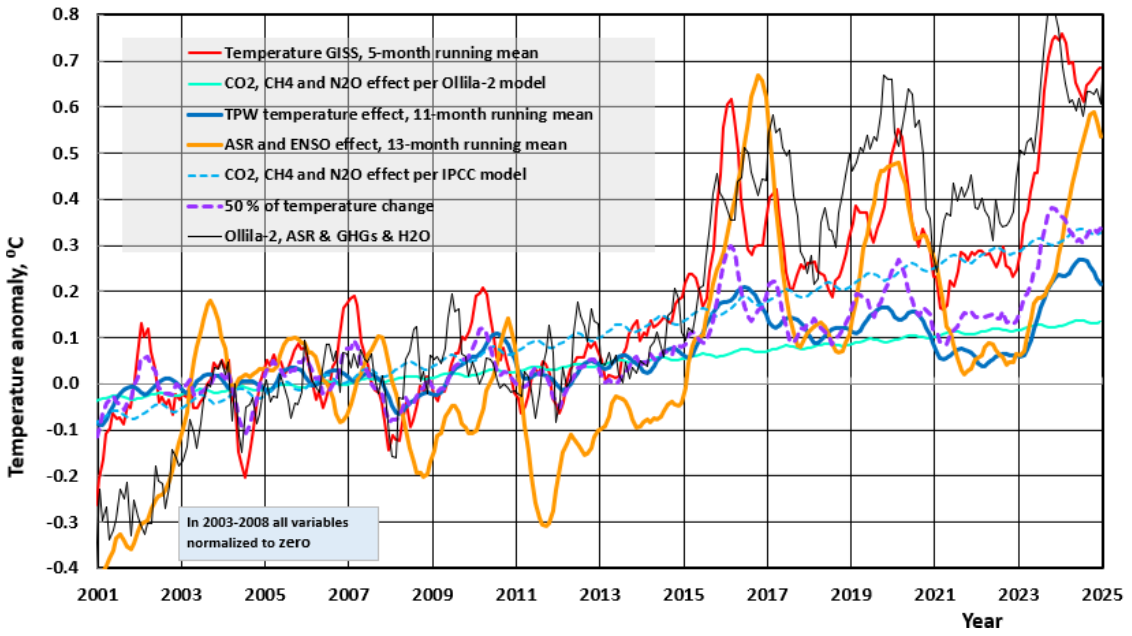

Figure 9: The temperature effects of CO_2, CH_4, and N_2O according to Ollila-2 (green solid curve) and IPCC models (dotted turquoise curve), water vapour (blue solid curve), and ASR+ENSO (brownish curve) have been depicted. The temperature anomaly (red curve) is according to the GISS (2025) data set calculated as a 5-month running mean. The lilac dotted curve illustrates the water vapour feedback effect caused by GH gases according to the C-C theory, which has doubled the original radiative forcings, and it is 50 % of the temperature curve. The warming impacts of ENSO have been calculated by Eq. (5). All variables have been normalised to zero in the period 2003-2008.

The theory in this study has been that the H_{TPW} variations depend on the primary energy changes, which were tested during the period from 2010 to 2025. The most important energy input is the ASR, which has increased by 2.01 Wm^{-2} from 2000 to the year 2023, which can be compared to the RF impact of 2.16 by CO_2 from 1750 to 2019 (IPCC 2021). The temperature effects of ASR and absolute humidity H_{TPW} have been illustrated in Fig. 10.

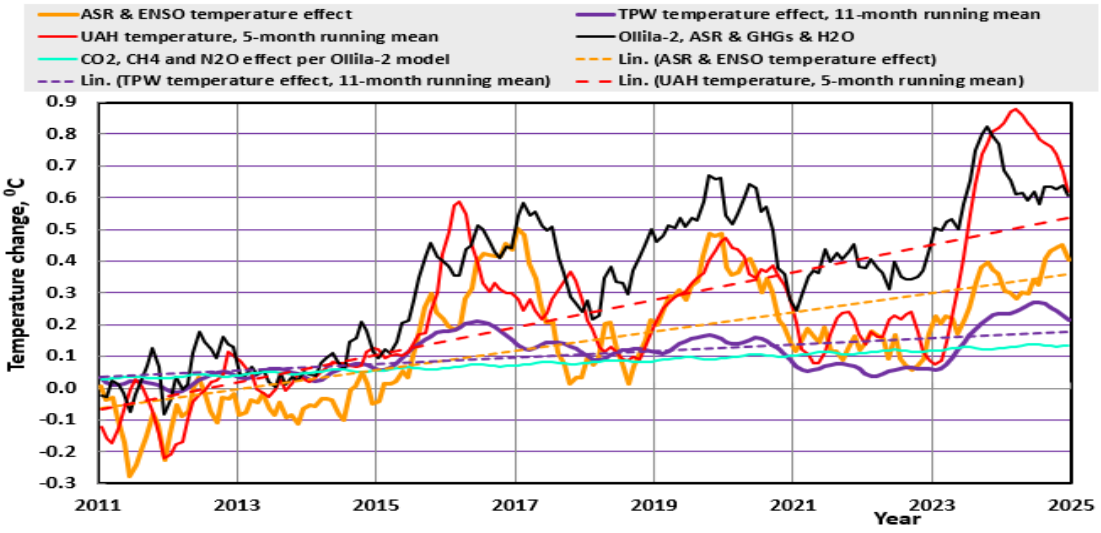

Figure 10: The trend curves of UAH temperature, the temperature simulations of the Ollila-2 model, and the temperature effects of TPW absolute humidity, ASR & ENSO, and GH gases by the Ollila-2 model from 2011 to 2025.

The H_{TPW} curve seems to correlate quite well with the ASR&ENSO curve. By judging with the eye, the H_{TPW} changes do not correlate with the impacts of GH gases. The multicorrelation coefficient of regression R^2 for the period 2005-2024 is 0.756 between the water vapour (H_{TPW}) and two variables, which are the temperature impacts of ASR&ENSO and the GH gases, according to the Ollila-2 model. The coefficient R^2 of the model with only ASR&ENSO is only slightly smaller, 0.688. It means that the H_{TPW} values depend mainly on ASR and ENSO, which are the primary energy inputs.

The linear increases of temperature and H_{TPW} temperature impacts from 2011 to 2025 are illustrated by the linear fittings of the actual trends in Fig. 10. The temperature increase has been 0.61 ºC, and the temperature increase of H_{TPW} impact has been 0.14 ºC, which means a 23 % feedback effect on the primary temperature drivers (mainly ASR and ENSO). It is more than 14 % as concluded from the ASR impacts during the seasonal temperature changes in section 4.3. A plausible explanation is that during the period 2011-2025, there have been two strong climate disturbances, namely two very strong El Niños: 2015-2016 with an ONI value of 2.64, and 2023-2024 with an ONI value of 1.95. As found by Ollila (2020), about 50 % of the temperature effect of very strong El Niños results from the 100 % water feedback effect during these short-term intervals of about one year. These two strong El Niños have increased the average water feedback during this short period from its normal level 14 % to an observed value of 23 %.

4.6 Temperature simulations of the 2000s

The temperature simulations during the 2000s have been carried out by applying the Ollila-2 model and the IPCC simple model (Fig. 11).

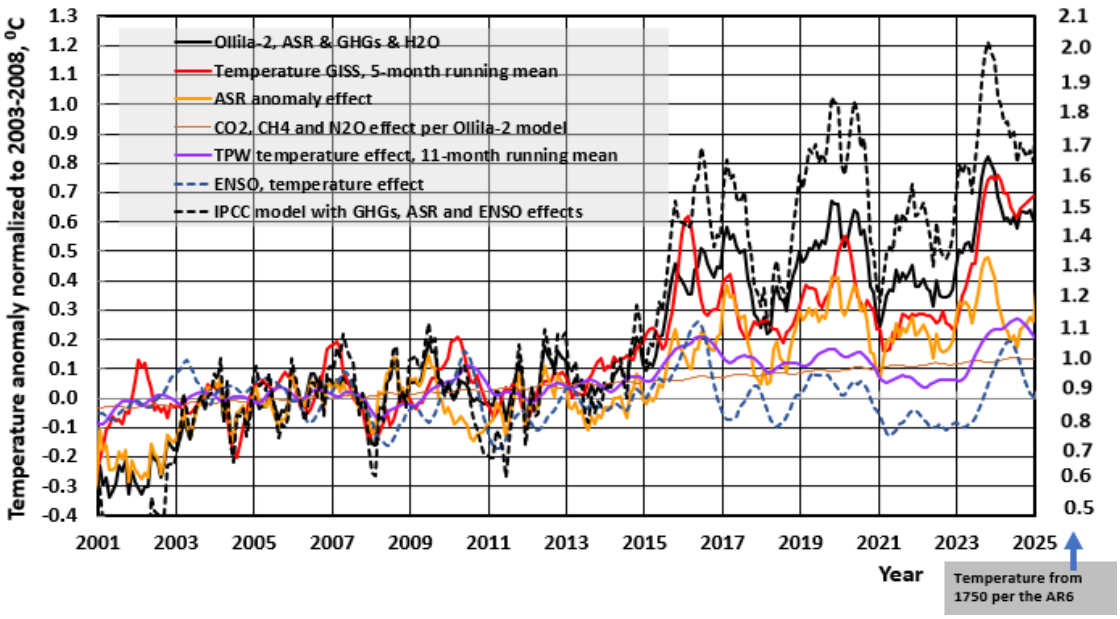

Figure 11: The graphs of the Ollila-2 model and GISS temperature from 2001 to 2025. The warming impacts of the three major climate drivers of ASR, GHGs, and TPW have been depicted for the same period according to the Ollila-2 model, as well as the ENSO according to Eq. (5). The dashed black curve is the simulated temperature response applying the λ-value of 0.47 K/(Wm^{-2}) according to the IPCC (2021).

The overall response of the Ollila-2 model is very good in comparison to observed temperature changes. By comparing the water vapour trend changes to the ENSO temperature changes, it is obvious that the major part of the ENSO effect happens through the changes in the atmospheric humidity and ASR changes. It can be noticed that the warming impacts of GH gases are very low. The ASR flux changes have had a major role in the temperature increase after the very strong El Niño in 2015-2016. The H_{TPW} values have stayed at a record level after the El Niño of 2023-2024, and it seems to be the main reason, besides the ASR, for the very high temperatures of 2023 and 2024.

The temperature effects of the Ollila-2 model are based on the calculated RF effects of climate drivers. The effect of GH gases is minimal according to the RF values of both the Ollila-2 and IPCC simple models. The simulated temperature by the IPCC model starts to deviate from the observed temperature after El Niño 2015-2016. The reason is the increased ASR anomaly. Since the water feedback theory implies that water content should have a similar impact as the original ASR impact, the result is a far too high temperature response.

It should be noted that nature cannot separate whether the ASR impact is due to solar radiation changes or the albedo changes. If these changes cause temperature increases, the water feedback theory of the IPCC implies that this mechanism doubles the temperature impact. The ASR increase from 2011 to 2019 was 1.29 Wm^{-2} according to CERES (2025) observations, which would increase the temperature by 0.6 ºC to about 1.9 ºC according to the IPCC science as described in section 1.3 (equation (3) with a λ value of 0.47 K/(Wm^{-2}). Maybe this is a reason why there is no ASR anomaly impact in Figure 7.7 of AR6, since the GCM-calculated temperature would deviate significantly from the observed: 1.9 ºC versus 1.29 ºC. Another good reason is that the GCMs are not capable of calculating an ASR impact through cloud property impacts on albedo. This problem becomes even more distinct when thinking that the aerosol and cloud effect has decreased from -0.82 Wm^{-2} in 2011 to -1.00 Wm^{-2} in 2019 in Fig. 7.7 (IPCC 2021), but the real effect has been significantly positive as noted above. By applying the real RF warming impact of water, the temperature follows the observed temperature very well.

The correlation coefficient of the Ollila-2 model to the observed GISS temperature from 2005 to 2024 is 0.82. The most realistic measure of the models is the Mean Absolute Error (MAE), which is calculated by the equation

$$\mathrm{MAE} = \mathrm{ABS}(\mathrm{d}T_O - \mathrm{d}T_C)/\mathrm{n}\ [\mathrm{Wm}^{-2}], \qquad (6)$$

where ABS is a function calculating the absolute error between the observed temperature anomaly T_O and the model-simulated temperature anomaly T_C, and n is the number of paired points. The MAE values calculated for the period from 2005 to December 2024 were 0.090°C for Ollila-2 and 0.183 °C for the IPCC model. These MAE values have been calculated from the original monthly values, even though the graphs in Fig. 10 have been smoothed by applying running mean values.

The greater MAE value of the IPCC model comes from the strong ASR flux increase after 2014, as noticed in Fig. 8, which overestimates the temperature response because of the water feedback

mechanism of this model.

5. Discussion and conclusions

Water vapour is the most important GH gas since it has a major role in the GH effect. This effect varies based on the studies from 50 % (Schmidt et al. 2010) to 89-95 % (Koutsoyiannis 2024), and on the other hand, the CO_2 effect also varies in broad limits from about 4 % - 5 % (Koutsoyiannis 2024) to 33 % (Pierrehumbert 2010) as surveyed in section 1.3. For some reason, the IPCC does not report these key figures at all. The RF value of the water vapour, depending on its concentration in the atmosphere, shows that it is practically linear in global concentrations without a strong decreasing RF effect like in the equation of CO_2. This feature explains why water's capability to absorb infrared radiation in the wavelength zone 12 μm to 19 μm almost nullifies the warming impact of increased concentration of CO_2 in the tropics. The RF value equation of water, based on the H_{TPW} values, gives the possibility to treat water concentration changes in the same way as the other GH gases.

A rather solid conclusion of this study is that the H_{TPW} value seems to depend on the primary energy variations of the Earth. During the relatively short period of 25 years of this study, the most important climate driver in this respect is the absorbed solar radiation (ASR) and its variations. The ENSO temperature impact acts in the same way as the ASR effect. Together, these two variables (ASR and ENSO) explain the temperature variations and the significant increase in temperature of the 2000s.

Water amplification could not be found in the case of GH gases, or it was insignificant, but only for the preliminary energy input changes, like ASR and ENSO. This result is not very solid concerning the warming impacts of GH gases, since during this short period, the GH impacts are very small. Anyway, the maximum water feedback is only 14 % and not about 100 % for any climate radiative forcing. In practice, the best and simplest way to factor in the water feedback is to use the RF calculation based on the H_{TPW} concentrations, since the water feedback is then automatically calculated according to its real impacts.

The ASR changes have been omitted in the GCM simulations of the AR6 (IPCC 2021) since these models have been constructed on the idea that ASR variations could be calculated through cloud property impacts. The simulation results of Ollila-2 simple climate models challenge the GCM models, which are based on the anthropogenic climate drivers only. Even though this is a short period, this model seems to give good results even when applied from the beginning of 1980.

In the year 2023, the global temperature increased about 0.28ºC, but the GH gases showed only an increase of about 0.02 ºC. Probably considering this fact, Schmidt (2024) wrote that GCMs cannot explain the high temperature of the year 2023, and it means that we are in uncharted territory. This study suggests two simple corrective measures applicable in all GCMs, which are the use of observed absorbed solar radiation (ASR) values and the concentration of water vapour for the calculation of the RF values in the same way as for other GH gases. In this way, the simulated temperatures are close enough to observations even by applying simple models.

The results of this paper challenge the water vapour feedback theory since the simulations show that the results using the RF of the water vapour are very good, instead of the water feedback theory of the C-C mechanism. It looks like the climate community is adhering to anthropogenic climate change, and they do not consider another paradigm, which leaves this question open for the time being.

Funding

No funds, grants, or other support were received.

Editor: Prof. Malamos**; Reviewers:** anonymous.

References

Bard E, Raisbeck G, Yiou F, Jouzel J, 2000: *Solar irradiance during the last 1200 years based on cosmogenic nuclides*. Tellus 52B:985–992. https://doi.org/10.1034/j.1600-0889.2000.d01-7.x

Bellouin N, Boucher O, Haywood J, Shekar Reddy M, 2003: *Global estimate of aerosol direct radiative forcing from satellite measurements.* Nature 438:1138-1141. DOI: 10.1038/nature04348

Berkley, 2025: *Temperature dataset*. https://berkeley-earth-temperature.s3.us-west-1.amazonaws.com/Global/Land_and_Ocean_complete.txt

CERES, NOAA, CERES EBAF-TOA Data, 2025: https://ceres-tool.larc.nasa.gov/ord-tool/jsp/EBAFTOA42Selection.jsp

Connolly R, Soon W, Connolly M, Baliunas S, Berglund J, Butler CJ, Cionco RG, Elias AG, Fedorov VM, Harde H et al. (2021): *How much has the Sun influenced Northern Hemisphere temperature trends? An ongoing debate*. Res. Astron. Astrophys. 21(6):131. https://iopscience.iop.org/article/10.1088/1674-4527/21/6/131?fbclid=IwaR0u-

Dewitte S, Cornelis J, Meftah M, 2022: *Centennial Total Solar Irradiance Variation*. Remote Sens. 14: 1072. https://doi.org/10.3390/rs14051072

Diamond MS, 2023: *Detection of large-scale cloud microphysical changes within a major shipping corridor after implementation of the International Maritime Organization 2020 fuel sulphur regulations.* ACP 23:8259–8269. https://doi.org/10.5194/acp-23-8259-2023

Gats, Gat Inc. 2025: *Spectral calculation tool*. https://www.spectralcalc.com/info/about

Gupta AK, Mittal T, Fauria KE, Bennartz R, Kok JF, 2022: *Hunga eruption cooled the southern hemisphere in 2022 and 2023.* Commun. Earth Environ. 6:240. https://doi.org/10.1038/s43247-025-02181-9

Harde H, 2014: *Advanced two-layer climate model for the assessment of global warming by CO_2.* Open Atm. Sc. J. 1(3):1-31. https://web.achive.org/web/20160429061756/http://www.scipublish.com/journals/ACC/papers/download/3001-846.pdf

Harde H, 2017: *Radiation Transfer Calculations and Assessment of Global Warming by CO_2.* Int. J. Atmos. Sci. 251034:1-30. https://doi.org/10.1155/2017/9251034

Harde H, 2022*: How Much CO2 and the Sun Contribute to Global Warming: Comparison of Simulated Temperature Trends with Last Century Observations.* Sci. Clim. Change. 2.2:105-133. https://doi.org/10.53234/scc202206/10

HITRAN, Harvard-Smithsonian Center for Astrophysics, 2024: *High-Resolution Transmission Molecular Absorption database*. https://www.cfa.harvard.edu/hitran/

Hodnebrog Ø, Myhre G, Jouan C, Andrews T, Forster PM, Jia H, Loeb NG, Olivié DJL, Paynter D, Quaas J, Raghuraman SP, Schulz M, 2024: *Recent reductions in aerosol emissions have increased Earth's energy imbalance.* Commun. Earth Environ. 5:166.

https://www.nature.com/articles/s43247-024-01324-8

Hoyt DV, Schatten KH, 1993*: A discussion of plausible solar irradiance variations, 1700-1992*. J. Geophys. Res.: Space Phys. 98:18895–906. https://doi.org/10.1029/93JA01944

Huang B, Angel W, Boyer T, Cheng L, Chepuring G et al., 2018: *Evaluation SST analyses with independent ocean profile observation.* J. Clim. 36: 5015-5030. DOI: https://doi.org/10.1175/JCLI-D-17-0824.1

Huang X, Chen X, 2020: *A synergistic use of hyperspectral sounding and broadband radiometer observations from S-NPP and Aqua.* Fall 2020 NASA Sounder Science Team Meeting, October 05.

IPCC, AR4, 2007: Climate Change 2007, The Physical Science Basis,_Cambridge Univ. Press, Cambridge, U.K., and New York. https://www.ipcc.ch/assessment-report/ar4/

IPCC, AR5, 2013: Climate Change 2013, The Physical Science Basis. Contribution of Working Group I to the Fifth Assessment Report of the Intergovernmental Panel on Climate Change. Cambridge Univ. Press, Cambridge, U.K., and New York. https://www.ipcc.ch/site/assets/uploads/2017/09/WG1AR5_Frontmatter_FINAL.pdf

IPCC, AR6, 2021: Climate Change 2021, The Physical Science Basis. Contribution of Working Group I to the Sixth Assessment Report of the Intergovernmental Panel on Climate Change. Cambridge Univ. Press, Cambridge, U.K., and New York. https://www.ipcc.ch/report/ar6/wg1/

ISCCP, The International Satellite Cloud Climatology Project, *FD data*, 2025. https://isccp.giss.nasa.gov/projects/flux/

Kiehl JT, Trenberth KE, 1997: *Earth's annual global mean energy budget*. Bull. Amer. Meteor. Soc 90: 311-323. DOI: https://doi.org/10.1175/1520-0477(1997)078<0197:EAGMEB>2.0.CO;2

Koutsoyiannis D, 2024: *Relative importance of carbon dioxide and water in the greenhouse effect: Does the tail wag the dog?* Sci. Clim. Change. 4.2:36-78. https://scienceofclimatechange.org/wp-content/uploads/SCC-Koutsoyiannis-DogTail-Nov-2024.pdf

Loeb NG, Thorsen TJ, Norris JR, Wang H, Su W, 2018: *Changes in Earth's energy budget during and after the "pause" in global warming: An observational perspective.* Climate 6, 62, https://www.mdpi.com/2225-1154/6/3/62

Loeb NG, Johnson GC, Thorsen TJ, Lyman JM, Rose FG, Kato S, 2021: *Satellite and ocean data reveal marked increase in Earth's heating rate.* Geophys. Res. Lett. 48, e2021GLO93047, https://doi.org/10.1029/2021GL093047

Ma N, Zhang Y, Yang Y, 2025: *Recent decline in global ocean evaporation due to wind stilling.* Geophys. Res. Lett. 5:e2024GL114256. https://doi.org/10.1029/2024GL114256

Manabe S, Wetherald RT, 1967: *Thermal equilibrium of the atmosphere with the given distribution of relative humidity*. J. Atm. Sci. 24(3):241-259. https://climate-dynamics.org/wp-content/uploads/2016/06/manabe67.pdf

Marsh ND, Svensmark H, 2000: *Low cloud properties influenced by cosmic rays.* Phys. Rev. Lett. 85(23), 5004–5007, DOI: https://doi.org/10.1103/PhysRevLett.85.5004

Matthes K, Funke B, Andersson ME, et al., 2017: *Solar forcing for CMIP6 (v3.2),* Geosci. Model Dev. 10:2247-2302. https://www.geosci-model-dev.net/10/2247/2017/gmd-10-2247-2017.pdf.

MetOffice, Met Office Hadley Centre, 2024: *Temperature data of HadCRUT5 and HadSST.4.1*. https://www.metoffice.gov.uk/hadobs/hadcrut5/data/HadCRUT.5.0.2.0/download.html

Mlawer EJ, Payne VH, Moncet J-L, Delamere JS, Alvarado MJ, Tobin DC, 2012: *Development and recent evaluation of MT CKD model of continuum absorption.* Philos. Trans. Math. Phys. Eng. Sci. A 370: 2520-2556. DOI: 10.1098/rsta.2011.0295

Meyssignac B, Chenal J, Loeb N, Guillaume-Castel R, Ribes A, 2023: *Time-variations of the climate feedback parameter λ are associated with the Pacific Decadal Oscillation*. Commun. Earth Environ. 4:241. https://doi.org/10.1038/s43247-023-00887-2

Nikolov N, Zeller NK, Roles of Earth's Albedo Variations and Top-of-the-Atmosphere Energy Imbalance in Recent Warming: New Insights from Satellite and Surface Observations. Geomatics 2024, 4(3), 311-341. https://doi.org/10.3390/geomatics4030017

NOAA, 2025a: *Pacific Decadal Oscillation (PDO).* https://psl.noaa.gov/pdo/

NOAA, Global Monitoring Laboratory (GML) of the National Oceanic and Atmospheric Administration, 2025b: *Web-based Reanalysis Intercomparison Tool: Monthly/Seasonal Time-Series.* https://psl.noaa.gov/data/atmoswrit/timeseries/index.html

NOAA, Global Monitoring Laboratory (GML) of the National Oceanic and Atmospheric Administration, 2025b: *Web-based Reanalysis Intercomparison Tool: Monthly/Seasonal Time-Series.* https://psl.noaa.gov/data/atmoswrit/timeseries/index.html0

NOAA, Global Monitoring Laboratory (GML) of the National Oceanic and Atmospheric Administration, 2025c: *Carbon dioxide, methane and nitrogen oxide concentrations*. https://gml.noaa.gov/ccgg/trends/

Ohmura A, 2001: *Physical Basis for the Temperature-Based Melt-Index Method*. J. Appl. Meteorol. Climatol. 40:754-76. DOI:https://doi.org/10.1175/1520-450(2001)040<0753:PBFTTB>2.0.CO;2

Ollila A, 2017: Warming effect reanalysis of greenhouse gases and clouds. PSIJ 13(2):1-13. https://journalpsij.com/index.php/PSIJ/article/view/374

Ollila A, 2019: The effect definition. PSIJ 23(2):1-5. https://doi.org/10.9734/psij/2019/v23i230149

Ollila A, 2020: *The pause end and major temperature impacts during super El Niños are due to shortwave radiation anomalies.* PSIJ 24(2):1-20. DOI: 10.9734/psij/2020/v24i230174

Ollila A, 2021: *Global Circulation Models (GCMs) simulate the current temperatures only if the shortwave radiation anomaly of the 2000s has been omitted*. Curr. J. App. Sci. Techn. 42(46):111-183. DOI: 10.9734/cjast/2021/v40i1731433

Ollila A, 2023a: *The 2023 record temperatures: correlation to absorbed shortwave radiation anomaly.* Sci. Clim. Change 4.1:74-87. DOI: 10.53234/scc202403/15

Ollila A, 2023b: *Radiative forcing and climate sensitivity of carbon dioxide (CO_2) fine-tuned with CERES data.* Curr. J. App. Sci. Techn. 40(17):45-52. DOI: 10.9734/cjast/2023/v42i464300

ONI, NOAA, 2025: *Oceanic Niño Index (ONI).* https://ggweather.com/enso/oni.htm

Pierrehumbert RT, 2010: *Infrared radiation and planetary temperature*. Phys. Today 64(1):33-

38.

Raghuraman SP, Soden B, Clement A, Vecchi G, Menemenlis S, Yang W, 2024: *The 2023 global warming spike was driven by the El Niño–Southern Oscillation*. Atm. Phys. Chem. 24:11275-112823.

Rantanen M, Laaksonen A, 2024: *The jump in global temperatures in September 2023 is extremely unlikely due to internal climate variability alone*. npj Clim. Atmos. Sci, 7:34.

Scafetta N, 2023: *Empirical assessment of the role of the Sun in climate change using balanced multi-proxy solar records.* GSF 14(6):101650. https://doi.org/10.1016/j.gsf.2023.101650

Schmidt GA, Ruedy RA, Miller RL, Lacis AA, 2010: *Attribution of the present-day total greenhouse effect.* J. Geophys. Res. 115:D20106. https://doi.org/10.1029/2010JD014287

Schmidt GA, 2024: *Climate models can't explain 2023's huge heat anomaly – we could be in uncharted territory*. Nature: 627. https://www.nature.com/articles/s41612-024-00582-9

Stefani F, 2021: *Solar and Anthropogenic Influences on Climate: Regression Analysis and Tentative Predictions*. Climate 2021, 9, 163. https://doi.org/10.3390/cli9110163

Stephens GL, Hakuba MZ, Kato S, Gettelman A, Dufresne J-L, Andrews T, Cole JNS, Willen U, Mauritsen T, 2022: *The changing nature of Earth's reflected sunlight*. Proc. R. Soc. A 478:20220053. https://royalsocietypublishing.org/doi/pdf/10.1098/rspa.2022.0053

Stine AR, Huybers P, Fung IY, 2009: *Changes in the phase of annual cycle of surface temperature*. Nature 457:435-441. https://www.nature.com/articles/nature07675

Svensmark H, 2019: *FORCE MAJEURE - The Sun's Role in Climate Change*, The Global Warming Policy Foundation, ISBN 978-0-9931190-9-5.

Trenberth KE, Fassullo JT, 2009: *Global warming due to increasing absorbed solar radiation.* Geophys. Res. Lett. 36: L07706. https://doi.org/10.1029/2009GL037527

Trenberth KE, Zhang Y, Fassullo JT, 2015: *Relationships among top-of-atmosphere radiation and atmospheric state variables in observations and CESM.* J. Geophys. Res. A. 120:10074-10090. https://doi.org/10.1002/2015JD023381

UAH, 2024: *Global temperature anomaly data set*. https://www.nsstc.uah.edu/data/msu/v6.0/tlt/uahncdc_lt_6.0.txt

Wang S, Xu T, Nie W, Jiang C, Yang Y, Fang Z, Li M, Zhang Z, 2020: *Evaluation of Precipitable Water Vapor from Five Reanalysis Products with Ground-Based GNSS Observations*. Remote Sensing, 12(11), 1817–1835. https://doi.org/10.3390/rs12111817

Wild M, Folini D, Schär C et al., 2013: *The global energy balance from a surface perspective.* Clim. Dyn. 40, 3107–3134. https://doi.org/10.1007/s00382-012-1569-8

Zhang T, Rossow WB, Lacis AA, Oinas V, 2004: *Calculations of radiative fluxes from the top of atmosphere based on ISCCP and other global data sets: Refinements of the radiative model and the input data*. J. Geo. Res. 109:1149-1165. https://doi.org/10.1029/2003JD004457

Appendix A. The average climate profiles applied in the LBL calculations

The climate zones are the five zones available in the Spectral Calculator application: tropical, midlatitude summer (ML-S), midlatitude winter (ML-W), polar summer (Polar-S), and polar winter (Polar-W). US Standard (US Stand) is the average atmospheric condition above the USA continent, and it has not been applied in these calculations. The weighing factors in calculating the average global profiles are 0.391 for the tropics, 0.461 for the midlatitude zone, and 0.148 for the polar zone. The profiles have been tabulated to the average altitude of 11 km of the troposphere, since thereafter the climate zone differences are insignificant, see Table A.1

Table A.1: Average global profiles 0 – 11 km altitude

Average global atmosphere - AGA			
Altitude	**Temperature**	**Pressure**	**Humidity**
km	Kelvin	mbar	g/m3
0	288.23	1013.90	11.06
1	283.68	900.23	7.36
2	278.84	797.91	5.16
3	274.45	705.34	3.33
4	268.29	622.01	2.10
5	262.00	547.05	1.24
6	255.58	479.54	0.67
7	249.10	418.88	0.36
8	242.58	364.78	0.16
9	236.31	316.37	0.05
10	230.36	273.62	0.01
11	226.02	235.71	0.00
		Total, prcm	**2.6**

Polar Summer (Polar-S) profiles have been applied in simulations. The water content of this climate profile has been adjusted by multiplying the profile values by 1.2384, which makes the total amount of precipitable water (prcm) 2.6 cm, which is the average water content of the atmosphere.

Appendix B. The capabilities of the Spectral Calculator

Ollila (2017) has calculated the global total absorption value using these five different climate zones to be 307.53 Wm^{-2} in the troposphere. The same value applying the adjusted Polar summer profiles is 305.98 Wm-2, which is only 0.5 % smaller. It can be estimated that this small difference does not affect RF calculations. Since the one profile calculation is so close to the five profile results, it is justifiable to use it in all LBL calculations in this study.

The Spectral Calculator LBL code, together with the HITRAN (2024) database, has been applied in numerous calculations without finding any problems or errors according to Gats (2024). The number of spectral lines originates from the HITRAN database, and spectra up to one million points can be calculated. The atmosphere is modelled as graduated concentric spherical shells. The number of shells depends on the path length and altitude range. For example, a path from the ground to 120 km (the top of our Spectral Calculator atmospheres) is split into 19 shells: 250 meters thick at the surface, growing to 10 km thick at high altitudes.

The author has applied this tool for calculating the CO_2 contribution in the GH effect by applying the US Standard Atmosphere 1976 with 12% water reduction, and the result is 27%, almost the same as the 26% calculated by Kiehl and Trenberth (1997) with the same atmospheric conditions. Schmidt et al. (2010) have calculated that the CO_2 contribution to the GH effect is 14 % corresponding to 21.7 Wm^{-2} absorption, and the same figures of the author applying the Spectral Calculator are 12.7 % / 20.1 Wm^{-2} using the GH effect magnitudes of 155 and 157.7 Wm^{-2}, respectively. Also, the total LW absorptions according to the altitude with the Spectral Calculator are the same as reported by Ohmura (2001): 1 km 90 %, 2 km 95 %, and 11 km 98 %.

The average global cloud layer is at an altitude from 1.5 km to 4.1 km (Wang et al., 2000), and the LW absorption by CO_2 has been completed below 1 km (Ollila, 2017). Thus, clear sky LW radiation reduction for a specific CO_2 concentration is accurate enough for the cloudy sky reduction, but the reduction of OLR flux due to cloud absorption is needed, which is proportional to OLR_{clear} according to the coefficient R_c.

Appendix C. The atmospheric conditions applied in the LBL calculations

In this study, the radiation flux of the clouds and the CERES (2024) data have been applied as reference material during the pause period from 2008 to 2014. This period has been selected since there are no exceptional climate events, and it is long enough for filtering out small deviations. The total precipitable water (TPW) amount has been 2.6 cm, carbon dioxide 393 ppm, methane concentration 1.803 ppm, and nitrogen oxide concentration 324 ppb at the surface level.

The surface-emitted LW flux is 398 Wm^{-2} according to the Earth's energy balance, applying the CERES radiation flux data (Wild et al., 2013). This flux value corresponds to Planck's temperature of 16.3 °C. Huang et al. (2018) have analysed five sea surface temperature (SST) datasets. During the pause from 2000 to 2014, the SST values varied from 18.1 °C to 18.5 °C. Since the oceans cover 70 % of the Earth's area, it means the real surface temperature is essentially higher than 15 °C, normally used as the global temperature estimate. The cloud fraction of this period has been 0.674 (CERES, 2024).

The average CERES observed OLR values in Wm^{-2} for this period are 240.038 for all-sky and 267.940 for clear sky, and the cloud fraction has been 0.674. The cloudy sky value is not readily available, but it can be calculated using the equation of Bellouin et al. (2003):

$$OLR_{all\text{-}sky} = 0.674 * OLR_{cloudy} + 0.326 * OLR_{clear} \qquad (a)$$

According to this equation, OLR for a cloudy sky is 226.54 Wm^{-2}. The clear sky flux of 268 Wm^{-2} at the TOA is the sum of 186 Wm^{-2} radiated from the atmosphere and 82 Wm^{-2} transmitted through the atmosphere. When the sky turns from a clear sky to a cloudy sky, the changes in radiation fluxes happen immediately. The transmittance flux of 82 Wm^{-2} disappears, and the atmosphere-radiated OLR of 226 Wm^{-2} becomes about 15.5 % smaller than the same of clear sky. This change is caused by the LW radiation absorption by clouds, which has an essential role in the GH effect.

The accurate ratio of OLR_{cloudy} to OLR_{clear} during the period 2008-2014 is 0.8455, which has been marked by R_c in this study. The author has used R_c in calculating the cloudy sky OLR values from the LBL calculated OLR_{clear} values, which are needed in RF calculations of CO_2.

The absorption effect of CO_2 happens below the 1 km altitude since the CO_2 is such a strong absorber in its waveband zone. The global surface temperature of cloudy sky conditions is about 0.1 °C higher than the all-sky conditions (Zhang et al., 2004). The explanation is that the reradiation from clouds increases more than the SW radiation to the surface decreases during relatively short periods of cloudy sky conditions (about two days of three are cloudy).